V European Conference on Computational Fluid Dynamics
ECCOMAS CFD 2010
J. C. F. Pereira and A. Sequeira (Eds)
Lisbon, Portugal,14-17 June 2010

COMPUTATIONAL MODELLING FOR CARDIOVASCULAR MEDICINE: PATIENT-SPECIFIC MODELLING OF ARTIFICIAL HEART VALVE HEMODYNAMIC PERFORMANCE

C. Wood[†], A. J. Gil[†], O. Hassan[†], S. S. Ashraf[‡]

[†]Civil and Computational Engineering Centre, Swansea University,
Singleton Park, Swansea, SA2 8PP, United Kingdom
e-mail: {c.wood,a.j.gil,o.hassan}@swansea.ac.uk
[‡]Cardiac Unit, Morriston Hospital
Swansea, SA6 6NL, United Kingdom
e-mail: saeed.ashraf@swansea-tr.wales.nhs.uk

Key words: Heart Valves, Cardiac Modelling, Fluid-Structure Interaction

Abstract. *This paper presents a state-of-the-art computational engineering methodology for the simulation of interacting fluids and solids, focusing specifically on applications within cardiothoracic medicine. We demonstrate that by harnessing powerful computational mesh generation, fluid and structural dynamics techniques, patient-specific models for realistic pre-operative surgical planning can be constructed for a range of surgical interventions, including artificial heart valves and ventricular assist devices, whilst also maintaining an acceptable turnaround time from the medical imaging stage to computational results. Considering the computational method, implicit coupling of the three-dimensional fluid and structure fields is achieved in a partitioned manner through the two-way transfer of information at the fluid-structure interface. Specifically, the time-dependent incompressible Arbitrary Lagrangian Eulerian Navier-Stokes equations are solved in finite volume manner using the artificial compressibility approach, with computational performance enhanced by an edge-based data structure, geometric multigrid and parallelisation. The dynamic nonlinear structure is solved using a finite element nonlinear hyperelasticity approach with Newton iteration and Newmark time integration scheme. In-house software for mesh generation, adaptation and local remeshing is utilised to maintain mesh quality throughout.*

To demonstrate the power of the method and the importance of using realistic, patient-specific geometric models, the numerical examples presented utilise a three-dimensional geometrical model of the left heart, extracted from real patient medical imaging data. Geometrical models of the intended surgical interventions, such as mechanical heart valves, are modelled in detail and incorporated into the geometric model of the patient's heart. Results from numerical fluid-structure interaction models demonstrate that the computational technique is capable of resolving complex flow features in the the surgically altered heart and therefore enables the hemodynamic flow characteristics of multiple cardiovascular surgical options to be compared preoperatively without any increased risk to the patient.

1 INTRODUCTION

The maturation of computational methods in fields once dominated by experimental testing, coupled with the growing affordability of computational resources, has stimulated increasing interest in more large-scale or multi-field areas of research. In recent years, Fluid Structure Interaction (FSI) problems in particular have received a great deal of attention from the computational mechanics community. Time-dependent problems involving large structural deformations have posed particularly challenging problems but offer a wide range of applications in the biomedical field. In cardiovascular medicine in particular, it is believed that a computational engineering analysis approach could enable an extremely detailed understanding of the fluid and structural dynamics processes at work in the cardiovascular system to be built up, with a level of detail at multiple scales well beyond that currently achieved through conventional experimental methods.

In-vivo and in-vitro experimental studies and more recently in-silico computational studies have yielded valuable information on the links between haemodynamic stresses and the problems such as blood damage and valve durability. However, for the power of computational techniques such Computational Fluid Dynamics (CFD) and Fluid Structure Interaction (FSI) to be relevant in Cardiovascular research, the numerical models and techniques adopted must be capable of considering with sufficient detail the great geometrical complexity of the heart structure as well as the widely varying range in temporal resolution required to fully capture the cardiovascular cycle.

Using the strongly-coupled partitioned fluid-structure interaction approach presented previously by the authors [3, 4], this paper will focus on the geometrically and physiologically accurate simulation of blood flow through a bileaflet mechanical heart valve. We will present the benchmark example of flow through a bileaflet mechanical valve mounted within a cylindrical tube and then demonstrate the dangerous shortcomings of assuming such a simplified model by demonstrating our latest anatomically accurate model of pulsatile blood flow through the left heart when a bileaflet mechanical valve is fitted in the mitral position. The resulting fluid-structure interaction analysis will be used to consider more realistically the effects of such surgical interventions in terms of patient recovery and the suitability of the artificial device.

2 MODEL CONSTRUCTION

2.1 Construction of mechanical device geometries

The geometrical description of the mechanical device may be constructed from manufacturers' CAD files or directly from a user-constructed geometry definition file which specifies curve components, surface components and surface region connectivity. Using the latter approach, a bileaflet mechanical valve geometry has been constructed using geometrical data provided in manufacturers' and current research literature and with reference to sample valve specimens available to us through collaborative links with medics

(a) ATS Open Pivot® Standard (b) Medtronic ADVANTAGE®

Figure 1: Typical bileaflet valves currently used in valve replacement surgery

at Swansea Morriston Hospital Cardiac Unit. High quality unstructured meshes have been generated using the in-house FLITE system [19], which features an efficient three-dimensional Delaunay triangulation procedure with automatic boundary point creation.

Specifically, the bileaflet valve model presented here seeks to replicate the most current bileaflet valve designs, such as ATS Open Pivot® Standard or Medtronic ADVANTAGE® depicted in Figure 1. Notably, these valves do not feature the protruding pivot guards typical of the widely studied St. Jude Medical® bileaflet mechanical valves. For a valve with tissue annulus diameter of 29mm the corresponding orifice inner diameter is taken as 24.8mm. The leaflets achieve an angle of 26° when closed and 89° when fully open, are of 1mm thickness and do not have any curvature. The hinge mechanisms of the leaflets, which can vary significantly depending upon the valve model and manufacturer, are not replicated.

2.2 Construction of an anatomically accurate heart geometry for CFD

A three-dimensional surface visualisation of the whole heart, constructed from high resolution MRI scan data by NYU School of Medicine and Zhang [20], shown in Figure 3(a),

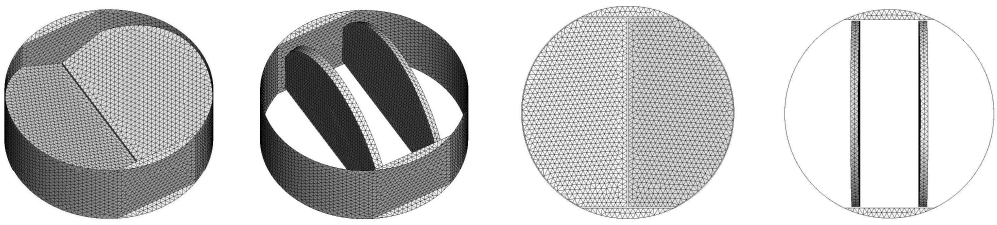

(a) Valve fully closed (b) Valve fully open (c) Valve fully closed (d) Valve fully open

Figure 2: Bileaflet mechanical valve model

is used as the starting point for the construction of an anatomically detailed geometrical model of the heart suitable for CFD and other forms of analysis. In order to generate a model suitable for the study of blood flow in the left side of the heart, the internal or "wet" surfaces corresponding to the left heart are extracted from the data set, Figure 3(b), and subjected to extensive remeshing and cosmetics procedures. We have used in-house unstructured mesh generation software throughout this procedure, including the correction of overlapping surface elements, improved resolution of desirable mesh features and increased mesh refinement, with the resulting improved mesh shown in Figure 3(c).

Areas of irretrievably poor resolution in the original scan data, such as the definition of the pulmonary veins, have been cleaned away to enable the merger of four idealised inflow tracts, featuring circular cross-sections of varying diameter, with the anatomic atrium surface geometry. The original idealised valve leaflet geometry definitions have also been removed in order to enable the insertion of geometries corresponding to the artificial valves under investigation. For convenience, the heart geometry is reorientated to align the mitral valve region with standard Cartesian axes. For examples involving the study of blood flow in the region of the mitral valve only the geometry of the aorta is terminated cleanly at the point where the aortic valve typically lies. Figure 3 illustrates the various stages in the construction of the model for the study of flow through the left heart and mitral valve region. The final boundary surface discretisation of triangular elements shown in Figure 3(d) forms the starting point for in-house tetrahedral or hybrid volume mesh generation software to perform the filling-in of the computational domain. The in-house software uses a fully automated Delaunay mesh generation procedure, as described in [19], with final mesh characteristics meeting user-defined mesh quality parameters through the use of cosmetic procedures such as diagonal swapping, element collapsing and Laplacian mesh smoothing. The final model of heart surfaces and volumetric discretisation are shown in Figures 3(d) and 3(e).

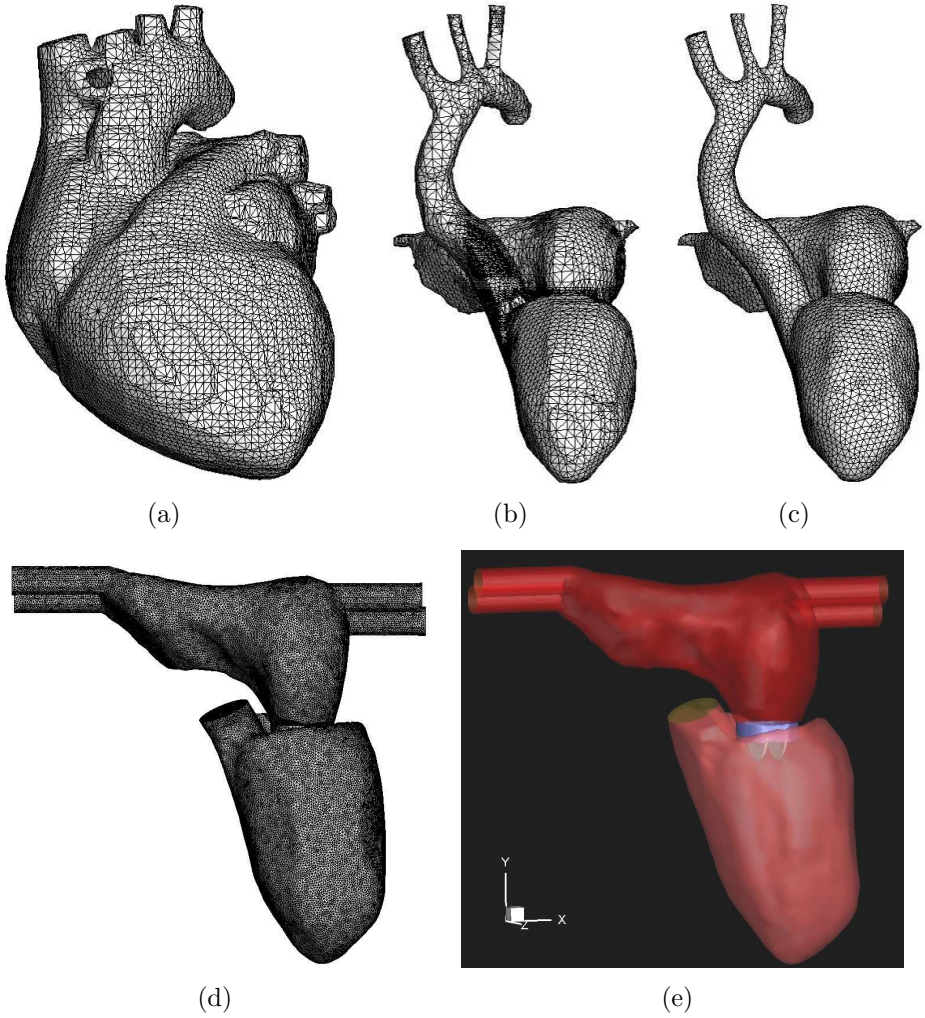

Figure 3: (a) Visualisation surface mesh of the whole heart, constructed from MRI scan data by NYU School of Medicine and Zhang [20] (b) Extracted internal surfaces of left heart - note the poor definition of pulmonary vein regions (c) Left heart surface mesh after mesh improvement (d) The reorientated left heart model with pulmonary vein inflow tracts, bileaflet mitral valve and aortic outflow (e) Heart model with transparent surface colouring

3 UNSTEADY INCOMPRESSIBLE FLUID FLOW WITH MOVING BOUNDARIES

The transient incompressible flow field is governed by the Navier-Stokes continuity and momentum equations. To improve the conditioning of the resulting hyperbolic system of equations, the artificial compressibility approach, first proposed by Chorin [5] and later extended by Turkel [6] is employed. The scheme features an implicit dual time stepping technique with explicit multi-stage Runga-Kutta time stepping in pseudo time and second order backwards differences in real time, within an Arbitrary Lagrangian-Eulerian formulation which enables unsteady flows with moving boundary components to be considered.

3.1 Governing Equations

With the development of an arbitrary Lagrangian Eulerian solution procedure in mind, the time-dependent Navier Stokes equations, modified by means of the artificial compressibility approach [5, 6], are considered in the integral form

$$\int_{\Omega(t)} \mathbf{P}^{-1} \frac{\partial \mathbf{U}}{\partial \tau} \mathrm{d}\Omega + \bar{\mathbf{I}} \frac{\mathrm{d}}{\mathrm{d}t} \int_{\Omega(t)} \mathbf{U} \mathrm{d}\Omega + \int_{\partial\Omega(t)} (\mathbf{F}_j - \bar{\mathbf{F}}_j) n_j \, \mathrm{d}S - \int_{\partial\Omega(t)} \mathbf{G}_j n_j \, \mathrm{d}S = \mathbf{0} \qquad (1)$$

over a time-dependent three dimensional domain $\Omega(t)$ bounded by a smooth closed surface $\partial\Omega(t)$. Here, n_j is the j^{th} component of the outward unit normal vector to $\partial\Omega$ of a cartesian coordinate system, t is the physical time whilst τ denotes pseudo time. The nondimensionalised vectors of unknowns $\mathbf{U}$, the inviscid, ALE and viscous fluxes $\mathbf{F}_j$, $\bar{\mathbf{F}}_j$ and $\mathbf{G}_j$ are given by

$$\mathbf{U} = \begin{bmatrix} p \\ u_1 \\ u_2 \\ u_3 \end{bmatrix} \quad \mathbf{F}_j = \begin{bmatrix} u_j \\ u_1 u_j + p\delta_{1j} \\ u_2 u_j + p\delta_{2j} \\ u_3 u_j + p\delta_{3j} \end{bmatrix} \quad \bar{\mathbf{F}}_j = \begin{bmatrix} 0 \\ u_1 \hat{u}_j \\ u_2 \hat{u}_j \\ u_3 \hat{u}_j \end{bmatrix} \quad \mathbf{G}_j = \begin{bmatrix} 0 \\ \tau_{1j} \\ \tau_{2j} \\ \tau_{3j} \end{bmatrix} \qquad (2)$$

where the standard summation convention on repeated indices is used and $j = 1, 2, 3$. In these expressions, ρ_F denotes the fluid density, u_j the component of the velocity vector in the direction x_j, p is the pressure, $\hat{u}_j$ is the velocity of the control volume boundary and δ_{ij} symbolises the Kronecker delta operator. Additionally, τ_{ij} are the components of the deviatoric stress tensor, formulated as

$$\tau_{ij} = \frac{1}{Re} \left(\frac{\partial u_i}{\partial x_j} + \frac{\partial u_j}{\partial x_i} \right) \qquad (3)$$

Finally, $\bar{\mathbf{I}}$ is a modified unit matrix and $\mathbf{P}$ is a preconditioning matrix for the pseudo-time equation system

$$\bar{\mathbf{I}} = \begin{bmatrix} 0 & 0 & 0 & 0 \\ 0 & 1 & 0 & 0 \\ 0 & 0 & 1 & 0 \\ 0 & 0 & 0 & 1 \end{bmatrix} \quad \mathbf{P} = \begin{bmatrix} \beta^2 & 0 & 0 & 0 \\ 0 & 1 & 0 & 0 \\ 0 & 0 & 1 & 0 \\ 0 & 0 & 0 & 1 \end{bmatrix} \tag{4}$$

where the parameter β can be viewed as a relaxation parameter for the pseudo-time solution procedure, with its value selected so as to optimise the convergence of the solution procedure [7]. Based upon numerical experiments, the value of β is defined as

$$\beta^2 = \max(\beta^2_{\min}, C_\beta |\mathbf{u}|^2) \tag{5}$$

with $\beta^2_{\min} = 1$ and $C_\beta = 2.5$.

3.2 Physical Time Discretisation

Following the discretisation of the physical time t, Equation (1) may be written in the form

$$[\mathbf{P}^m]^{-1} \int_{\Omega(t)} \frac{\mathrm{d}\mathbf{U}}{\mathrm{d}\tau}\bigg|^m \mathrm{d}\Omega + \bar{\mathbf{I}} \frac{\mathrm{d}}{\mathrm{d}t} \int_{\Omega(t)} \mathbf{U}|^m \,\mathrm{d}\Omega + \int_{\partial\Omega(t)} \left(\mathbf{F}^m_j - \bar{\mathbf{F}}^m_j - \mathbf{G}^m_j\right) n_j \,\mathrm{d}S = \mathbf{0} \tag{6}$$

where the superscript m denotes an evaluation at time $t = t^m$. The three level, second order, backward difference representation for a control volume $\Omega_I(t)$

$$\frac{\mathrm{d}}{\mathrm{d}t} \int_{\Omega_I(t)} \mathbf{U}|^m \,\mathrm{d}\Omega = \frac{1}{\Delta t} \left(\frac{3}{2} \Omega^m_I \mathbf{U}^m - 2\Omega^{m-1}_I \mathbf{U}^{m-1} + \frac{1}{2} \Omega^{m-2}_I \mathbf{U}^{m-2} \right) = \mathscr{T}\left(\mathbf{U}^m\right) \tag{7}$$

is employed for the approximation of the physical time derivative, where $\Delta t = t^{m+1} - t^m$ denotes the physical time step.

3.3 Dual mesh construction

To develop a cell vertex finite volume method for the spatial discretisation of the governing equations, identification of a dual mesh is required. This dual mesh, illustrated in Figure 4, is constructed by connecting edge midpoints, element centroids and face centroids of the basic tetrahedral fluid mesh, in such a way that only one node is contained within each dual mesh cell. The dual mesh cells then form the control volumes for the subsequent finite volume algorithm. Equation (6) is then applied to each dual mesh volume in turn. For the sake of brevity, we develop here only the form of the discrete equation at interior nodes I of the mesh. For a more detailed presentation of the algorithm, References [8, 9, 10, 11] may be consulted.

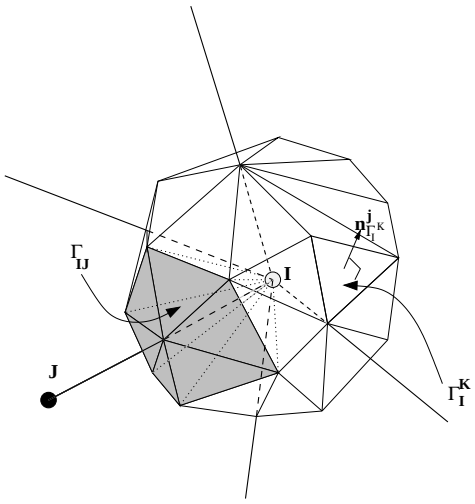

Figure 4: The dual mesh surrounding an internal node I.

3.4 Treatment of the inviscid and viscous fluxes

To evaluate the approximation of the integral an edge-based implementation is adopted in which the coefficients for each edge are calculated by using the dual mesh segment associated with the edge. For an internal edge connecting nodes I and J, these coefficients are computed as

$$\mathscr{C}^m_{j,IJ} = \sum_{K \in \Gamma_{IJ}} A^m_{\Gamma_I^K} \, n_j^{\Gamma_I^K,m} \tag{8}$$

where $A^m_{\Gamma_I^K}$ is the area of facet Γ_I^K and $n_j^{\Gamma_I^K,m}$ is the jth component of the unit unit normal vector to the facet from the viewpoint of node I at time level m.

Then, assuming the integrand is constant over the segment, and equal to its value at the midpoint of the edge, the inviscid and viscous flux terms are approximated as

$$\int_{\partial\Omega_I^m} \left(\mathbf{F}^m_j - \mathbf{G}^m_j\right) n_j \mathrm{d}S = \sum_{J \in \Lambda_I} \frac{\mathscr{C}^m_{j,IJ}}{2} \left[\left(\mathbf{F}^m_{j,I} + \mathbf{F}^m_{j,J}\right) - \left(\mathbf{G}^m_{j,I} + \mathbf{G}^m_{j,J}\right)\right] \tag{9}$$

where Λ_I denotes the set of all nodes connected to node I by edges in the mesh. From equations (2) and (3), it is apparent that the evaluation of $\mathbf{G}^m_{j,I}$ and $\mathbf{G}^m_{j,J}$ requires the evaluation of the gradients. At a typical interior node I, these derivatives are obtained, by again using the approach adopted above, as

$$\left.\frac{\partial u_i}{\partial x_j}\right|^I = \frac{1}{\Omega_I} \sum_{J \in \Lambda_I} \frac{\mathscr{C}_{j,IJ}}{2} (u_{i,I} + u_{i,J}) \tag{10}$$

which results in a second order accurate discretisation with a non-compact computational stencil which stretches over five points.

3.5 Treatment of the ALE fluxes

An important property of Equation (1) is geometric conservation. The Geometric Conservation Law (GCL), first shown in [12], requires that the control-volume movement itself has no direct effect on the fluxes, in the sense that if the unknown field is constant, the numerical solution does not change in time in the presence of a moving mesh, i.e. from Equation (1)

$$\frac{\mathrm{d}}{\mathrm{d}t}\int_{\Omega(t)} \mathrm{d}\Omega - \int_{\partial\Omega(t)} \hat{u}_j\, n_j \, \mathrm{d}S = 0. \tag{11}$$

It is desirable to retain this quality numerically, after discretisation. This has led to the so-called Discrete Geometric Conservation Law (DGCL), as advocated in [14, 15, 16], which governs the geometric parameters of the numerical scheme, such as grid positions and velocities, so that the corresponding numerical scheme reproduces exactly a constant solution.

The numerical integration of the ALE fluxes is performed in the usual way by summing the edge contribution, with the ALE edge coefficient $\mathscr{D}_{IJ}^m$ introduced such that

$$\int_{\partial\Omega_I^m} \bar{\mathbf{F}}_j^m n_j \, \mathrm{d}S = \sum_{J\in\Lambda_I} \frac{\mathscr{D}_{IJ}^m}{2}\left(\bar{\mathbf{U}}_I^m + \bar{\mathbf{U}}_J^m\right), \tag{12}$$

where $\bar{\mathbf{U}} = [0, u_1, u_2, u_3]^T$. The task of finding ALE coefficients that render the scheme geometrically conservative is not trivial and has been treated by a number of authors [12, 13, 14, 15, 16]. Here the approach of [13] is followed. From Equation (11), it can be stated that in order to maintain geometric conservation at a discrete level, the change in volume of a moving cell I must be equal to the volume swept by the its boundaries from time t^m to t^{m+1}

$$\Omega_I^{m+1} - \Omega_I^m = \int_{t^m}^{t^{m+1}} \int_{\partial\Omega_I(t)} \hat{u}_i\, n_i \, \mathrm{d}\Omega \, \mathrm{d}t \tag{13}$$

Assuming that the mesh moves in a linear fashion between time levels t^m and t^{m+1}, a local geometric conservation law expressing the change in volume due to the movement of a triangular facet Γ_I^K between time levels t^m and t^{m+1} can be written as

$$\delta\, V_{\Gamma_I^K}^{m+1,m} = \Delta\, t \hat{u}_i^{\Gamma_I^K,*} n_i^{\Gamma_I^K,*} A_{\Gamma_I^K}^* \tag{14}$$

where $\hat{u}_i^{\Gamma_I^K,*}$ is the average facet velocity, $A_{\Gamma_I^K}^*$ is the average facet area and $n_i^{\Gamma_I^K,*}$ is the average normal. This term can be recognised as the contribution to the numerical ALE

coefficient of a single facet multiplied by the time step. Summing over all the facets of the boundary surface of the control volume connected to the edge IJ yields the expression for the edge-based ALE coefficient for a first order discretisation in time as

$$\mathscr{D}_{IJ}^{m+1} = \frac{1}{\Delta t} \sum_{K \in \Gamma_{IJ}} \delta \; V_{\Gamma_I^K}^{m+1,m} \tag{15}$$

If the second-order time discretisation given in Equation 7 is applied, however, a modified version of the ALE flux must be employed to ensure discrete geometric conservation. The modification

$$\hat{\mathscr{D}}_{IJ}^{m+1} \;\; = \;\; \frac{3}{2}\mathscr{D}_{IJ}^{m+1} - \frac{1}{2}\mathscr{D}_{IJ}^{m}$$

is adopted [17] which makes the numerical ALE coefficient second order in time. In addition, velocity boundary conditions at the moving boundary are applied as

$$\mathbf{u}_I^{w,m+1} = \frac{1}{\Delta t}(\mathbf{x}_I^{m+1} - \mathbf{x}_I^{m}) \tag{16}$$

if a first-order in time scheme is used or

$$\mathbf{u}_I^{w,m+1} = \frac{1}{\Delta t}(\frac{3}{2}\mathbf{x}_I^{m+1} - 2\mathbf{x}_I^{m} + \frac{1}{2}\mathbf{x}_I^{m-1}) \tag{17}$$

if the second order backwards difference in time scheme is used, which is consistent with the dual mesh velocity definition.

3.6 Solution procedure

If $\mathscr{S}_{j,IJ}\,(j = 1, 2, 3)$ denotes the components of a unit vector in the direction of the vector $\mathscr{C}_{j,IJ}$, equation (6) may be re-expressed as

$$\Omega_I \frac{\mathrm{d}\mathbf{U}_I^m}{\mathrm{d}\tau} = \mathcal{R}_I^m \tag{18}$$

where

$$\mathcal{R}_I^m = \bar{\mathbf{I}}\mathscr{T}(\mathbf{U}_I^m) - \mathbf{P}_I^m \sum_{J \in \Lambda_I} \left\{ \frac{\mathscr{C}_{IJ}^m}{2} \left[(\mathscr{F}_I^m + \mathscr{F}_J^m) - (\mathscr{G}_I^m + \mathscr{G}_J^m) \right] - \frac{\mathscr{D}_{IJ}^m}{2} \left(\bar{\mathbf{U}}_I^m + \bar{\mathbf{U}}_J^m \right) \right\} \tag{19}$$

and

$$\mathscr{F}_I = \mathscr{S}_{j,IJ}\mathbf{F}_{j,I}, \qquad \mathscr{G}_I = \mathscr{S}_{j,IJ}\mathbf{G}_{j,I}, \qquad \mathscr{C}_{IJ} = (\mathscr{C}_{j,IJ}\mathscr{C}_{j,IJ})^{1/2} \tag{20}$$

At each physical time level $t = t_m$, the value of $\mathbf{U}^m$ is obtained by integrating Equation (18) in pseudo–time to steady state, using an explicit three stage Runga–Kutta scheme. A stable computational procedure is achieved by the explicit of an artificial

viscosity term, constructed in the Jameson-Schmidt-Turkel manner [18]. Parallelisation of the solution algorithm is implemented by the domain decomposition multigrid approach (DD-MG) using the Single Program Multiple Data(SPMD) parallel architecture with the Message Passing Interface(MPI) model for communication of data. A more detailed description of the solution procedure as well as verification of the robustness of the algorithm may be found in the References [9, 10, 8, 11].

4 MODELLING THE DYNAMIC MOTION OF THE HEART AND VALVE

4.1 Cardiac Modelling Methodologies

Research seeking to capture the dynamic motion of the heart or valves has classically stemmed from the fields of both biology and engineering. Research stemming from computational engineering modelling has typically addressed the structural mechanics and fluid dynamics components of the action of the heart and a great many computational methods, primarily based upon FSI coupling, have now been developed for this purpose. These range from boundary-fitted approaches originating from the field of aeroelasticity, which utilise highly developed field-specific fluid and structure solvers [21, 22], to interface capturing approaches such the Fictitious Domain method and similar [23, 24, 25, 26] and the Immersed Boundary methodologies [27, 28]. Many of these cardiac models are concerned with investigating blood ejection from the heart and therefore focus on the flows induced by the contraction of the left ventricle, using simple geometries with and without the mitral and aortic valves. Another very active area of research is that of mechanical valve performance, particularly dealing with reproducing anatomic-quality blood flow characteristics in the ventricle and blood damage arising from phenomena such as high wall shear stresses and cavitation during valve closure.

Research coming from the computational systems biology field has typically addressed modelling the electrophysiological cellular activation and structural mechanics phenomena specific to heart tissue. Four decades of experimental and computational research have led to the development of cellular models for all of the main types of cardiac myocyte (cardiac muscle cells) [29] and the current state of the art in biophysical cardiac modelling now lies in the development of computational methods for the efficient coupling of these cardiac cell models to three–dimensional cardiac electromechanics models [30, 31]. Weakly coupled models have been presented for idealised left ventricle geometries and validated against experimental data [32] and although strong coupling methodologies are believed to yield a more accurate representation of the electrical activation–active tension–structural deformation coupled phenomena in the heart, the significant increase in computational workload has meant that such models have thus far only been made possible by implementing greatly simplified cell or structural mechanics models, or models with a very basic geometry [30].

Investigation of medical devices has great potential for commercial exploitation as well as medical impact, and in 1998 the EU funded project BloodSim [33] investigated the develop-

ment of commercial software for biomedical applications. Whilst the majority of models seeking to replicate heart valve function continue to neglect the expansion/contraction behaviour of the ventricular walls, computational engineering research is now being carried out with more realistic representations of the surrounding heart and chordae, notably in [28], who consider a novel design for an artificial chorded mitral valve. The model presented here aims to accurately capture key stages of the cardiac cycle including mitral valve opening, ventricular expansion and mitral valve closure, all within the context of an anatomically-based geometrical model. Extensive experimental testing of mechanical valve characteristics is documented in the literature by authors such as [35, 34] and it is upon this data that this work has currently based the opening/closure characteristics of the mitral valve.

4.2 Prescribed Leaflet and Ventricle Action

Specifically, at the beginning and end of the diastolic phase the valve leaflets rotate between an angle of 0°, corresponding to fully closed, to an angle of 63°, corresponding to fully open, over a period of 0.05 seconds in a nonlinear fashion, displayed in Figure 5. Upon valve opening, ventricular filling begins and fluid flows from the pulmonary vein inflows and the atrium into the ventricle, increasing the volume of blood in the ventricle from 50mL to 120mL over a period of 0.5 seconds. In order to satisfy incompressibility within the fluid, the velocity of fluid prescribed at the inflows is varied at each timestep according to a prescribed variation in ventricular volume at that timestep. The correspondence between the valve opening and closure and the variation in ventricular volume is displayed in the graph in Figure 6.

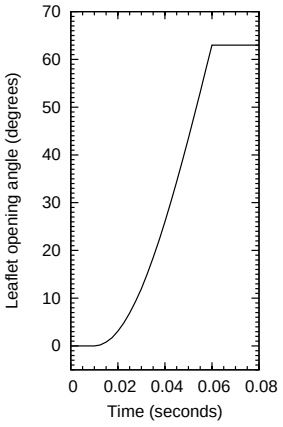

(a) Leaflet motion during opening

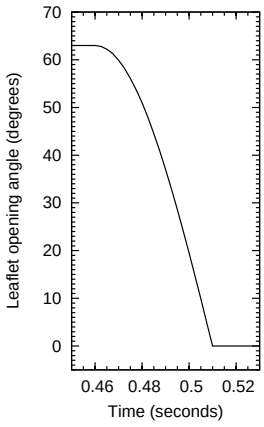

(b) Leaflet motion during closure

Figure 5: Valve leaflet opening/closing characteristics

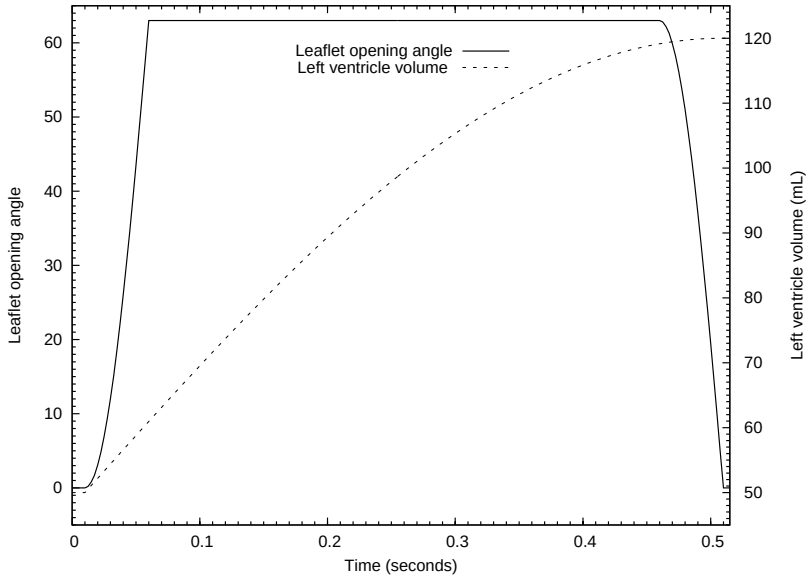

Figure 6: Leaflet opening angle and corresponding volume of blood in the left ventricle

5 SOLUTION PROCEDURE

At each timestep the heart and valve geometry must conform to a prescribed leaflet angle and ventricular volume, according to Figure 6. Therefore, at each timestep a corresponding inflow velocity must be calculated in order to satisfy incompressibility within the fluid. In addition, ALE coefficients corresponding exactly to the motion of the boundary surfaces must be calculated in order to correctly model the fluid flow. In order to simplify these stages in the analysis and minimise error in the fluid solution, all of the boundary surface nodes maintain a fixed connectivity, though changing coordinates. In contrast, the coordinates and connectivity of the internal points within the mesh are capable of being modified significantly during the analysis. The positions of both the boundary and the internal nodes are first moved according to a spring analogy in order to accommodate the prescribed boundary displacement. Then, if the volume mesh quality falls below set parameters, regions of the interior mesh can be subjected to a local remeshing scheme, as described in [19]. If remeshing does take place then fluid field solution data pertaining to the old mesh is interpolated onto the new mesh using a linear interpolation scheme. A flowchart outlining the overall scheme is shown in Figure 7.

6 NUMERICAL EXAMPLES

6.1 Flow through a bileaflet valve mounted within a cylindrical pipe - flow phenomena at valve closure

The bileaflet valve described previously and pictured in figure refvalvemeshes is mounted within a long tube of circular cross section. At the pipe inlet a parabolic inflow velocity

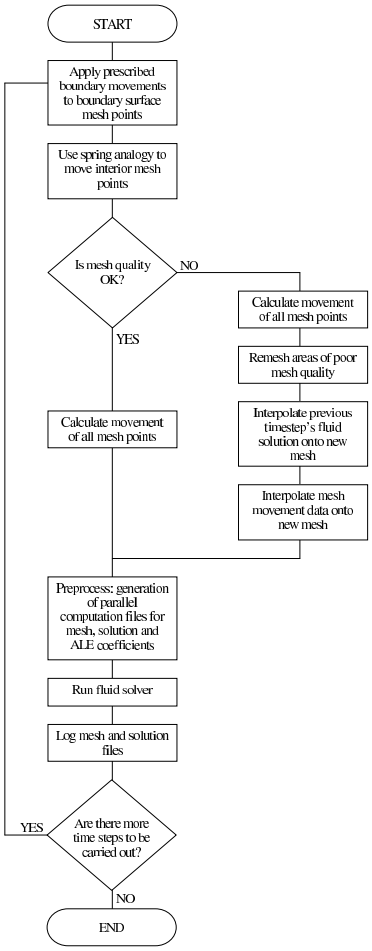

Figure 7: Flowchart of the solution process

distibution is applied, with peak flow of 36.58mm/s at the centre of the pipe and flow velocity of zero at the pipe walls.

Such models are often constructed, both computationally and experimentally, for the testing of artificial heart valve characteristics. The assumption of a straight tube at both the inlet and outlet of the valve is a fair assumption for the study of aortic valve physiologies, but comparison of this example with flows in Example 2 will seek to demonstrate that such a simplified geometry is not relevant in the study of mitral valve haemodynamics.

As can be observed in Figure 8, fluid flow within the pipe upstream and downstream of the valve is symmetric and laminar and in the immediate region of the valve symmetry is also maintained.

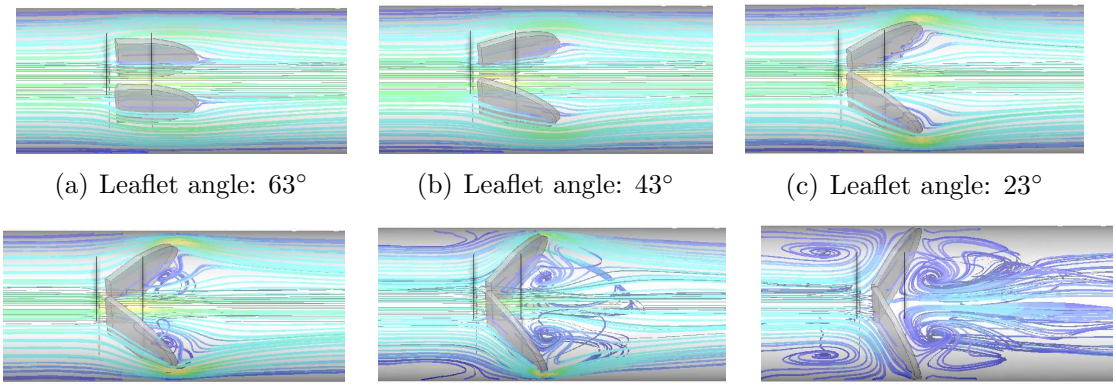

(a) Leaflet angle: 63° (b) Leaflet angle: 43° (c) Leaflet angle: 23°

(d) Leaflet angle: 12° (e) Leaflet angle: 4° (f) Leaflet angle: 2°

Figure 8: Fluid flow characteristics through a bileaflet valve mounted within a cylindrical pipe at closure.

6.2 Pulsatile flow through a bileaflet valve mounted in the mitral position of an anatomically realistic left heart

In this example, mitral valve opening, left ventricular filling and mitral valve closure are all considered within one computational simulation of the diastolic component of the cardiac cycle. The variation of valve leaflet angle at opening and closure is prescribed according to experimental data, as explained previously in section 4.2. Ventricular volume change due to filling corresponds to a stroke volume of $70 \times 10^3 mm^3$ and the pulsatile variation in the inflow velocity at the four pulmonary vein inflow boundaries is determined according to this volume change in order to ensure the fluid incompressibility condition is maintained.

Streamlines of the fluid flow characteristics are pictured at key stages of the simulation in Figure 9. It can clearly be seen that the fluid within the atrium is highly chaotic and not at all like the Poiseuille pipe flow demonstrated in Example 1. As the valve leaflets open, high velocity jets of fluid can be seen between the valve housing and the edges of the leaflets, with a jet of somewhat velocity flow through the central channel. These fluid jets initially impact strongly on the lower left hand wall of the ventricle. However, the rapid expansion of the ventricle downwards and outwards towards the right hand side of the body leads to highly non-symmetric, somewhat rotational flow within the ventricle.

At the end of the diastolic phase, the valve leaflets rapidly close upwards. In Figures 9(n), 9(o) and 9(p) regions of very high velocity gradient can clearly be noted, particularly at the leaflet tips. These observations correspond with the widespread medical research which considers high velocity gradients at valve closure to be a significant contributing factor towards the red blood cell damage that is strongly associated with mechanical heart valves.

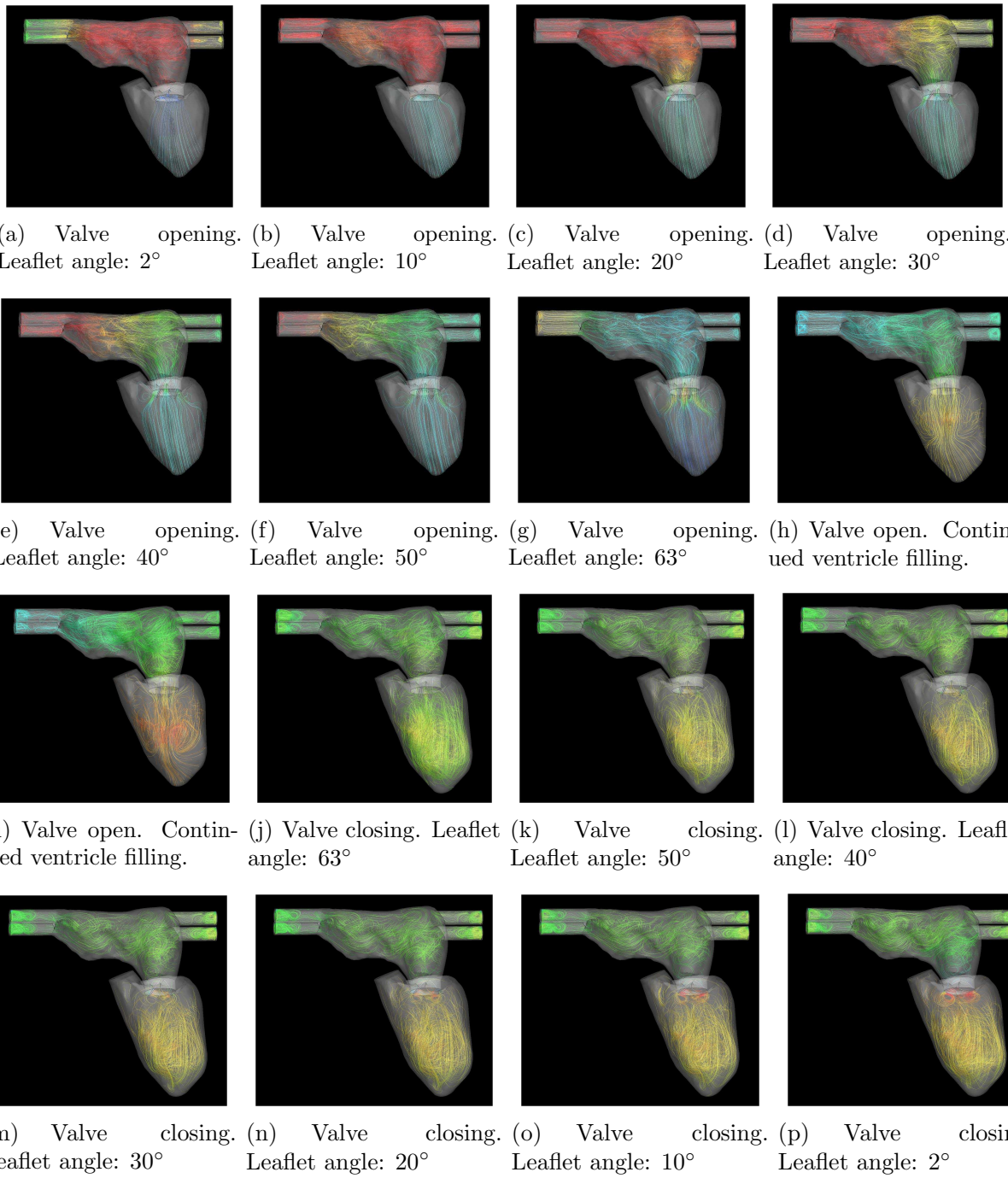

(a) Valve opening. Leaflet angle: 2°
(b) Valve opening. Leaflet angle: 10°
(c) Valve opening. Leaflet angle: 20°
(d) Valve opening. Leaflet angle: 30°
(e) Valve opening. Leaflet angle: 40°
(f) Valve opening. Leaflet angle: 50°
(g) Valve opening. Leaflet angle: 63°
(h) Valve open. Continued ventricle filling.
(i) Valve open. Continued ventricle filling.
(j) Valve closing. Leaflet angle: 63°
(k) Valve closing. Leaflet angle: 50°
(l) Valve closing. Leaflet angle: 40°
(m) Valve closing. Leaflet angle: 30°
(n) Valve closing. Leaflet angle: 20°
(o) Valve closing. Leaflet angle: 10°
(p) Valve closing. Leaflet angle: 2°

Figure 9: Fluid flow characteristics during the valve opening, ventricle filling and valve closure phases.

7 CONCLUSIONS

The realistic heart geometry which has been developed herein has been shown to be capable of being adapted for the study of implanted haemodynamic devices, specifically an artificial heart valve implanted in the mitral valve position. In studying the standard example of a bileaflet valve mounted within a cylindrical pipe against the realistic heart model, it has been clearly demonstrated that the fluid flow characteristics in the region of the valve and the downstream flow are extremely different in the two cases. Therefore, we can conclude that future study of mitral valve haemodynamics must take into account the physiology of both the atrium and ventricle for realistic results to be obtained.

Thus, at this first stage, the realistic heart model and the partitioned computational strategy utilised has proven to be robust and flexible to work with. Future work will address improved modelling of important physiological features, such as chordae tendineae and the development of models for native heart valves in healthy and diseased states.

REFERENCES

[1] British Heart Foundation Statistics Website http://www.heartstats.org [19 October 2009]

[2] Thourani VH, Weintraub WS, Guyton RA, Jones EL, Williams WH, Elkabbani S and Craver JM Outcomes and Long-Term Survival for Patients Undergoing Mitral Valve Repair Versus Replacement: Effect of Age and Concomitant Coronary Artery Bypass Grafting *Circulation* 2003;**108**:298-304; DOI:10.1161/01.CIR.0000079169.15862.13

[3] Wood C, Gil AJ, Hassan O and Bonet J Partitioned block Gauss-Seidel coupling for dynamic fluid-structure interaction *Computers and Structures* 2008; DOI:10.1016/j.compstruc.2008.08.005

[4] Wood C, Gil AJ, Hassan O and Bonet J A partitioned coupling approach for dynamic fluid-structure interaction with applications to biological membranes *Internation Journal of Numerical Methods in Fluids* 2008; DOI: 10.1002/fld.1815

[5] Chorin AJ, A numerical method for solving incompressible viscous flow problems *Journal of Computational Physics* 1967;**2**:12–26.

[6] Turkel E Preconditioned methods for solving the incompressible and low speed compressible equations, *Journal of Computational Physics* 1987;**72**:277–298.

[7] Rizzi A and Eriksson LE, Computation of inviscid incompressible flow with rotation *Journal of Fluid Mechanics* 1985;**153**:275–312.

[8] Sørensen KA, A multigrid accelerated procedure for the solution of compressible fluid flows on unstructured hybrid meshes, Ph.D. thesis, University of Wales Swansea, 2001.

[9] Gil AJ, Zhang Z, Hassan O and Morgan K A parallel unsteady multigrid des algorithm for the solution of 3D incompressible flows on unstructured grids *Journal of Aerospace Engineering* 2006; **19**: 271–280.

[10] Hassan O, Sørensen KA, Morgan K and Weatherill NP A method for time accurate turbulent compressible fluid flow simulation with moving boundary components employing local remeshing *Internation Journal of Numerical Methods in Fluids* 2007;**53**:1243–1266.

[11] Zhang Z, Gil AJ, Hassan O and Morgan K The simulation of 3D unsteady incompressible flows with moving boundaries on unstructured meshes *Computers and Fluids.* 2008; DOI: 10.1016/j.compfluid.2007.07.013

[12] Thomas PD and Lombard CK, Geometric conservation law and its application to flow computations on moving grids *AIAA Journal* 1979;**17**:1030–1037.

[13] Nkonga B. and Guillard H Godunov type method on non-structured meshes for three-dimensional moving boundary problems *Computer Methods in Applied Mechanics and Engineering* 1994;**113**;183–204.

[14] Lesoinne M, Farhat C and Maman N Geometric conservation laws for problems involving moving boundaries and deforming meshes, and their impact on aeroelastic computations *Computer Methods in Applied Mechanics and Engineering* 1996;**134**; 71–90.

[15] Koobus B and Farhat C Second-order time-accurate and geometrically conservative implicit schemes for flow computations on unstructured dynamic meshes *Computer Methods in Applied Mechanics and Engineering* 1999;**170**; 103–129.

[16] Farhat C, van der Zee KG and Geuzaine PH Provably second-order time-accurate loosely-coupled solution algorithms for transient nonlinear computational aeroelasticity *Computer Methods in Applied Mechanics and Engineering* 2001;**195**;1973–2001.

[17] Venkatakrishnan V and Mavriplis DJ Implicit method for the computation of unsteady flows on unstructured grids *Journal of Computational Physics* 1996;**127**, 380–397.

[18] Jameson A, Schmidt W and Turkel E Numerical simulation of the Euler equations by finite volume methods using Runge-Kutta timestepping schemes *AIAA Aerospace Sciences Meeting* 1981; (AIAA-1981-1259).

[19] Weatherill NP and Hassan O Efficient three-dimensional Delaunay triangulation with automatic boundary point creation and imposed boundary contraints *International Journal of Numerical Methods in Engineering* 1994;**37**:2005–2039.

[20] Zhang Y, Bajaj C and Sohn BS 3D finite element meshing from imaging data *Computer Methods in Applied Mechanics and Engineering* 2004;**194**:5083–5106.

[21] A. Redaelli et al, *3D simulation of the St. Jude medical bileaflet valve opening process: Fluid-structure interaction study and experimental validation*, J. Heart Valve Dis. **13** (2004), 804–813.

[22] C. Guivier et al, *New insights into the assessment of the prosthetic valve permormance in the presence of subaortic stenosis through a fluid-structure interaction model*, J. Biomech. **40** (2007), 2283–2290.

[23] J. De Hart et al, *A three-dimensional computational analysis of fluidstructure interaction in the aortic valve*, J. Biomech. **36** (2003), no. 1, 103–112.

[24] K.S. Einstein et al, *Non-linear fluid-coupled computational model of the mitral valve*, J. Heart Valve Dis. (2005), 376–385.

[25] K.S. Kunzelman et al, *Fluid-structure interaction models of the mitral valve: function in normal and pathological states*, Phil. Trans. **262** (2007), 1393–1406.

[26] R. van Loon et al, *A fluid-structure interaction method with solid/rigid contact for heart valve dynamics*, J. Comp. Phys. **217** (2006), 806–823.

[27] C.S. Peskin et al, *Cardiac fluid dynamics.*, Crit. Rev. Biomed. Eng. **20** (1992), 451–459.

[28] P.N. Watton et al, *Dynamic modelling of prosthetic chorded mitral valves using the immersed boundary method*, J. Biomech. **40** (2007), 613–626.

[29] D. Noble, *Systems biology: The genome, legome and beyond*, Science **295** (2002), 1678–1682.

[30] S.A. Niederer et al, *An improved numerical method for strong coupling of excitation and contraction models in the heart*, Progr. Biophys. Mol. Biol. **96** (2008), 90–111.

[31] J. Sainte-Marie et al, *Modeling and estimation of the cardiac electromechanical activity*, Computers and Structures **84** (2006), 1743–1759.

[32] R.C.P. Kerckhoffs et al, *Electromechanics of paced left ventricle simulated by straighforward mathematical model: comparison with experiments*, American Journal of Physiology **289** (2005), 1889–1897.

[33] D.R. Hose et al, *Fundamental mechanics of aortic heart valve closure*, J. Biomech. **39** (2006), 958–967.

[34] Cheng R, Lai YG and Chandran KB Three-dimensional fluid-structure interaction simulation of bileaflet mechanical heart valve flow dynamics *Annals of Biomedical Engineering* 2004 ; **32**:14711483

[35] Lai YG, Chandran KB and Lemmon J A numerical simulation of mechanical heart valve closure fluid dynamics *Journal of Biomechanics* 2002 ; **35**:881-892

[36] Einstein DR, Del Pin F,Jiao X, Kuprat AP, Carson JP, Kunzelman KS, Cochran RP, Guccione JM and Ratcliffe MB. Fluid-structure interactions of the mitral valve and left heart: Comprehensive strategies, past, present and future. *Communications in Numerical Methods in Engineering* 2009 ; DOI:10.1002/cnm.1280

[37] Nakamura M, Wada S and Yamaguchi T Influence of the opening mode of the mitral valve orifice on intraventricular haemydynamics *Annals of Biomedical Engineering* 2006 ; **34**:927-935 ; DOI: 10.1007/s10439-006-9127-3

[38] Yoganathan A, Chandran KB and Sotiropoulos F Flow in Prosthetic Heart Valves: State-of-the-Art and Future Directions *Annals of Biomedical Engineering* 2005 ; **33**:1689-1694 ; DOI: 10.1007/s10439-005-8759-z

[39] van Loon R, Anderson PD and van de Vosse FN A fluid-structure interaction method with solid-rigid contact for heart valve dynamics *Journal of Computational Physics* 2006 ; **217**:806-823 ; DOI: 10.1016/j.jcp.2006.01.032.